Neck formation and role of particle-particle contact area in the thermal conductivity of green and partially sintered alumina ceramics

David Smith, Jorge Martinez Dosal, Siham Oummadi, Delphine Nouguier, Diana Vitiello, Arnaud Alzina, Benoit Nait-Ali

Version of Record: https://www.sciencedirect.com/science/article/pii/S0955221921008414
Manuscript_0873cda0ebec01b8e397e0aa8c124da9

Neck formation and role of particle-particle contact area in the thermal conductivity of green and partially sintered alumina ceramics

David S. Smith*, Jorge Martinez Dosal, Siham Oummadi, Delphine Nouguier, Diana Vitiello, Arnaud Alzina, Benoit Nait-Ali

University of Limoges,

Institute of Research for Ceramics (UMR CNRS 7315)

87068 Limoges, France

Abstract:

Sintering ceramics involves neck formation, densification and eventually grain growth. A simplified model is developed to describe the effects of pore fraction, average grain size and the contact area between particles due to neck formation on the thermal conductivity of the green or partially sintered ceramic. Laser flash measurements on green bodies of alumina powders with different average particle sizes reveal similar thermal conductivity values close to 0.5 $Wm^{-1}K^{-1}$, corresponding to thermal resistances for equivalent planes of contacts in the range 10^{-7} to 2 10^{-6} m^2KW^{-1}. BET specific surface area measurements were then used to estimate the contact area due to neck formation in partially sintered alumina ceramics fired from 400°C to 1200°C. As predicted by the model, there is a strong increase in thermal conductivity. Such information is relevant as input data for numerical modelling of the green body behaviour during thermal treatment.

Keywords: alumina ceramics; green bodies; thermal conductivity; sintering; neck formation.

* Corresponding author. E-mail: david.smith@unilim.fr

1 Introduction

Fabrication of ceramic products typically involves preparation of the raw material as a powder, forming the basic shape of the ceramic body, drying and then firing at high temperature. It is through the sintering mechanisms taking place in the ceramic green body during the firing step that mechanical strength and the final dimensions of the ceramic article are achieved. Two important aspects of the firing step are the energy cost and the thermal response time of the green body. These are determined by the thermophysical characteristics of the ceramic green body: heat capacity, thermal conductivity and the body dimensions. Since the ceramic material exhibits strongly different microstructures before and after firing, these characteristics change significantly during the process. Variation in the volume heat capacity is principally controlled by densification, which can be evaluated by dilatometric measurements, in association with values of specific heat (heat capacity per unit mass) available for simple oxides in thermochemical data handbooks. The current work is therefore focused on the evolution of the thermal conductivity from the initial powder compact (green body) to the fired ceramic.

A ceramic green body, which is formed by pressing, typically contains 45-50% porosity. This porosity will decrease the overall thermal conductivity due to the low thermal conductivity of air (0.026 $Wm^{-1}K^{-1}$ at room temperature) which is much less than the solid phase. However the packed particles of the green body present another feature affecting overall thermal conductivity. The particle – particle contacts offer significant thermal resistance and the contact area is initially small. Consequently the measured thermal conductivity of a ceramic green body is low compared to a fired dense ceramic [1,2]. A typical value for an alumina green body is 0.6 $Wm^{-1}K^{-1}$ which can be compared to greater than 30 $Wm^{-1}K^{-1}$ for large grain dense alumina [2,3]. Heat treatment of the pressed powder compact during firing induces three major sintering mechanisms: formation of necks with well-defined grain boundaries between particles, densification with elimination of porosity and grain growth. Each type of modification to the microstructure influences the overall thermal conductivity; generally by an increase.

Olorunyoleni et al. studied ZnO ceramic green bodies with measurements of the thermal diffusivity by the laser flash technique for thermal treatments up to 600°C [1]. This maximum temperature was chosen to avoid densification and consequently an increase in the observed thermal conductivity values was attributed to neck formation between particles. With similar concerns Poulier et al. chose to study tin oxide green bodies [4]. Due to the predominance of surface diffusion in this material, pressed powder compacts of pure tin oxide present the advantage for study of almost no densification when subjected to thermal treatment even at 1500°C. Neck formation between particles is initiated already at 200°C so that a thermal treatment at 500°C was sufficient to increase the thermal conductivity by a factor of 4 before grain growth takes place. In another approach using an in-situ device to measure thermal diffusivity and sample dimensions simultaneously, Raether and Springer demonstrated an increase in thermal diffusivity of alumina pressed powder compacts by a factor of 5 or more attributed to neck formation before densification sets in above 1000°C [5].

From a theoretical point of view, starting from Coble's two-sphere sintering model which describes neck growth through surface diffusion, Birnboim et al. used a numerical 3D model to predict the evolution of effective thermal conductivity of a ZnO green body during a heating/cooling cycle between room temperature and 600°C [6,7]. Recently, Uhlirova et al.

examined the thermal conductivity and Young's modulus of partially sintered alumina ceramics from the perspective of pore shape [8]. They used numerical simulation to predict the changes in these properties when the pore shape evolves from concave to convex; corresponding to the sintering process. If these approaches give the broad features of the behavior for the green body, they do not explicitly take the interface thermal resistance at particle – particle contacts into account. Presumably, both the nature, implying the value, of the thermal resistance of particle-particle interfaces at the microscopic scale (corresponding to just solid – solid contacts) and the contact area of these particle – particle interfaces can evolve. The aim of the present paper is to give further insight into these aspects and their role in the effective thermal conductivity of a ceramic green body without entering into the interesting debate of the validity or not of minimum solid area models for porous materials [9,10].

Pressed powder compacts of alumina have been chosen for study due to their high intrinsic thermal conductivity and technological importance. The concept of an equivalent plane of contacts as the predominant contribution in the thermal response is introduced. A simplified model for the effective thermal conductivity of the ceramic body with an evolving microstructure is proposed for interpretation of experimental data. The values of effective thermal conductivity at room temperature for pressed powder compacts with different average particle sizes (or granulometries) are measured using the laser flash technique. Analysis is made to calculate the thermal resistance of an equivalent plane of contacts and the effect of the number of contacts in the plane is discussed. Then, the evolution of the room temperature thermal conductivity of the green body due to heat treatment is examined. In particular, for treatments before major densification sets in, this is related to the changes in microstructure in terms of particle – particle contact area as revealed by BET measurements. Analysis using the simplified model gives information on the thermal resistance of the particle – particle contacts.

2 Experimental

Materials

Pressed compacts in disc form of alumina were prepared by uniaxial pressing of commercial powders in a 13 mm diameter die. The table below summarizes the product source, an estimate of the average grain size from SEM observations and relative density of the green body.

Table 1

Characteristics of alumina ceramic green bodies.

Alumina powder	Supplier	Average grain size	Relative density (%)
TM-DAR	Tamei chemicals	0.16 μm	55
AKP30	Sumitomo chemicals	0.25 μm	55
P172SB	ALTEO	0.39 μm	54
P152SB	ALTEO	0.71 μm	60
AR12	ALTEO	1.25 μm	43
Aldrich	Aldrich	2.9 μm	57
AC34	ALTEO	3.0 μm	56

An estimate of the relative density of each pressed powder compact was made from the dry weight and measurement of the disc dimensions.

Microstructure

Scanning electron microscope observations were made with two instruments: a Cambridge S260 SEM and a JEOL JSM 7400F FEG. For these porous samples average grain diameters were estimated directly using the software measurement bar on populations of typically 50 grains. BET specific surface area measurements were made on the starting powders, green bodies and thermally treated samples using a Micromeritics Tristar II 3020 instrument.

Thermal conductivity

Room temperature measurements of thermal diffusivity (α) were made with a Netzsch LFA 427 Laser-flash device or an older laboratory made setup. In either case the accuracy for the values of α is generally within 3% related to measurement reproducibility and evaluation of sample thickness. Prior to measurement, sample discs were coated with graphite on both faces, in order to enhance the absorption of the laser energy and improve the back face signal emission. Once the value of thermal diffusivity is extracted from the measured temperature-time data, the thermal conductivity (λ) is calculated with the expression.

$$\lambda = \alpha \rho C_p \qquad (1)$$

where ρ is the sample density, and C_p is the specific heat from literature [11].

The evaluation of α from the temperature-time behaviour was performed using Degiovanni's analysis or the Cape Lehman model which both take into account heat losses from the disc sample [12,13]. No significant radiation effects were detected. Uncertainty in conductivity values was assessed to be less than ± 5%.

3. Theory

3-1 Thermal resistance for an equivalent plane of particle – particle contacts

After pressing of the starting powder, the microstructure of the ceramic green body consists typically of a well packed assembly of grains containing 45 – 50% porosity. Fig. 1(a) shows the micrograph of a fine grain alumina green body, following a thermal treatment at 400°C; just sufficient to initiate neck formation between particles but not alter the grain or pore arrangement. Positions for some of the particle – particle contacts are indicated in the frame of Fig. 1(b).

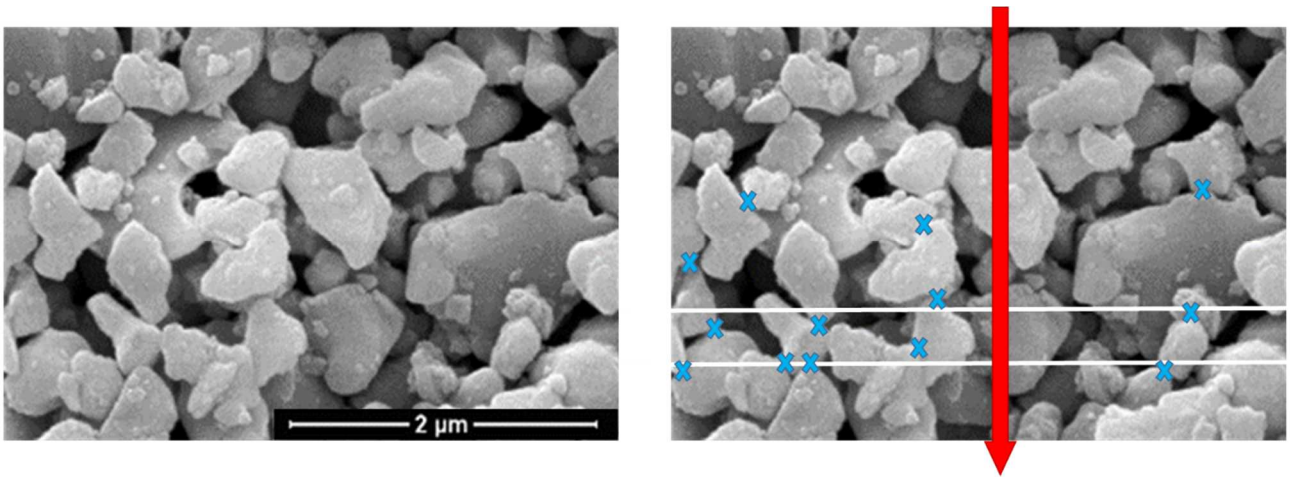

Fig. 1 (a) Micrograph of an alumina green body treated at 400°C. (b) Identification of grain – grain contact points (blue crosses) and two planes perpendicular to a heat flow direction.

The thermal resistance of the interface between particles in mechanical contact will be greater than a well formed grain boundary after neck formation. Furthermore, before sintering is initiated, the real contact area between particles is small and the particle – particle interface resistance is assumed to have a dominant effect on the overall thermal conductivity of the green body. For linear heat flow, the thermal resistance of the green body can be simplified to a number of equivalent planes of particle – particle contacts, like the ones depicted in Fig. 1(b), connected in series. In reality the equivalent planes have a slight thickness to accommodate variations in the packing of particles in the assembly and consequently in the particle – particle contact positions. The equivalent planes are separated by a distance given by the average grain size as illustrated in the idealized microstructure in **Fig. 2**. In a first instance, the thermal resistance of the grains is assumed to be negligibly small compared to the contact interfaces.

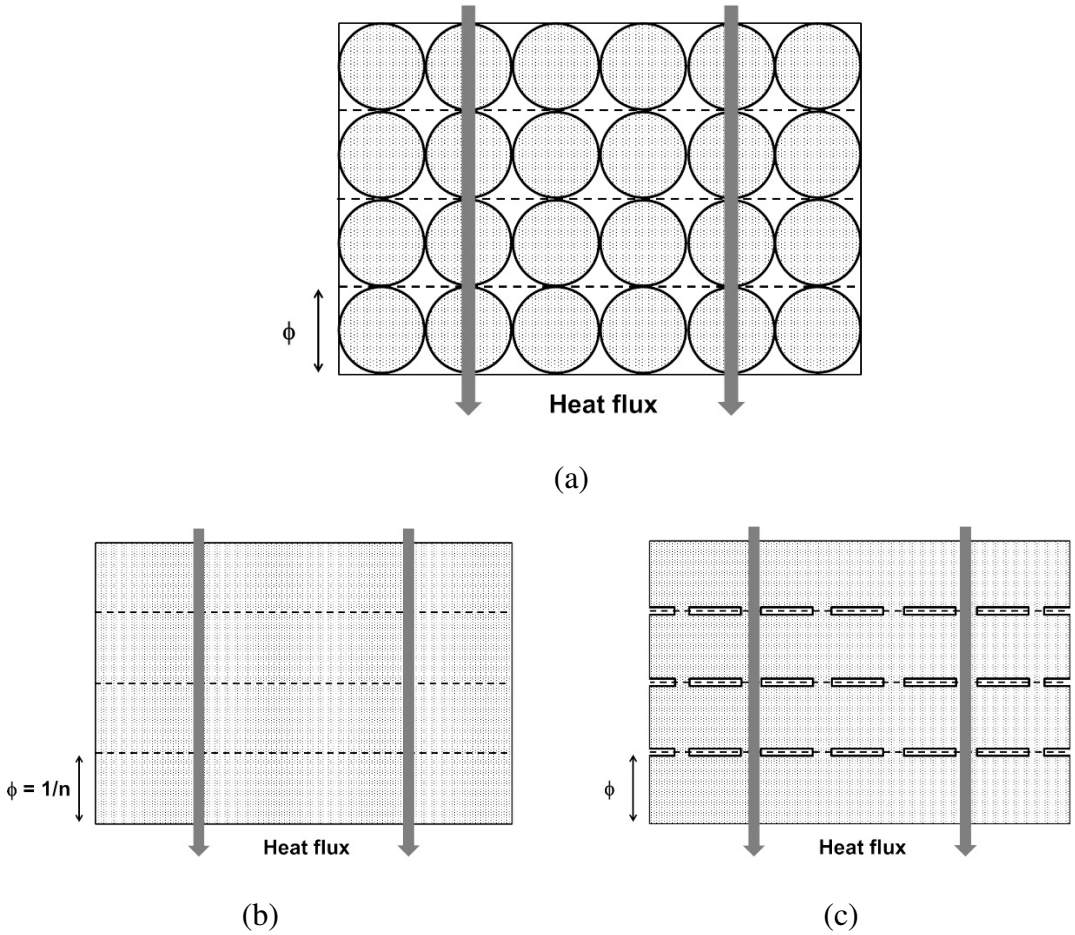

Fig. 2: (a) Green body represented as an idealized arrangement of pores and particles with small solid-solid contact area. The arrows indicate the heat flow through the sample. (b) Equivalent solid phase portion of green body approximated by flat slabs separated by interface planes. (c) Equivalent solid matrix for the green body where interface planes exhibit both reduced area solid-solid contacts and narrow gaps of empty space.

3-2 Simplified model for effective thermal conductivity of ceramic green body

The construction of a model for the effective thermal conductivity of a green or partially sintered ceramic needs to take into account contact area between the particles, pore volume fraction and average particle size. All these parameters can vary with heat treatment during sintering. We develop a simple relation in three steps as illustrated in **Fig. 2.**

The green body is represented in a simplified manner as rows of touching particles with neighbouring voids (i.e. pores) due to the packing arrangement and particle shape as shown in **Fig. 2(a)**. In the first step the green body is divided into a fictive solid phase with conductivity λ_s and the pore phase. For convenience, the thermal conductivity is described by Landauer's relation [14] given by:

$$\lambda = \frac{1}{4}\left[\lambda_p(3v_p - 1) + \lambda_s(2 - 3v_p) + \left(\left[\lambda_p(3v_p - 1) + \lambda_s(2 - 3v_p)\right]^2 + 8\lambda_s\lambda_p\right)^{1/2}\right] \quad (2)$$

where $v_p$is the pore volume fraction and λ_p is the pore thermal conductivity. The choice of Landauer's relation is motivated by its success for describing the thermal conductivity of sintered ceramics containing open porosity [15]. Though the situation in the green body may not be identical, the approach permits to compare green bodies containing different amounts of porosity. By assigning $\lambda_p = 0$ as a simplification, due to the small value of the conductivity ratio for pore and solid phases, Eq.(2) can be written:

$$\lambda = \lambda_s\left(1 - \frac{3}{2}v_p\right) \quad (3)$$

In the next step the fictive solid phase, represented in **Fig. 2(b)**, is considered as a series of particle – particle contact planes with thermal resistivity given by

$$\frac{1}{\lambda_s} = \frac{1}{\lambda_{grain}} + nR_{int} \quad (4)$$

where λ_{grain} is the grain thermal conductivity, n is the number of contact planes per unit length of heat path related to the inverse grain size and R_{int} is the thermal resistance of the particle – particle contact plane. Eq. (4) is similar to the approach adopted for describing the thermal conductivity of dense polycrystalline alumina ceramics [3]. By assuming that $nR_{int} >> \frac{1}{\lambda_{grain}}$ and that $n = 1/\phi$ where ϕ is the average grain size, then

$$\frac{1}{\lambda_s} \approx \frac{R_{int}}{\phi} \quad (5)$$

In the 3rd step, the thermal resistance of an equivalent plane of contacts in the green body is examined as it evolves with thermal treatment. Two contributions acting in parallel carry heat across the plane. These are the particle – particle interfaces in mechanical contact corresponding to the initial green body and those particle – particle interfaces which have formed necks with grain boundaries at the contact due to sintering as depicted in **Fig. 2(c)**. The combined resistance of an equivalent plane of contacts can be written as:

$$\frac{1}{R_{int}} = \left(\frac{S'}{S}\right)\frac{1}{R'_{int}} + \left(1 - \frac{S'}{S}\right)\frac{1}{R''_{int}} \quad (6)$$

where R'_{int} is the grain boundary thermal resistance in the neck with contact area S', R''_{int} is the thermal resistance of zones of particle – particle interfaces just in mechanical contact. S is the cross sectional area of the fictive solid phase. As sintering progresses with thermal treatment,

the contact area $S'$of the particle – particle necks increases whereas the area of the original mechanical contacts decreases as given by $\left(1-\frac{S'}{S}\right)$. A final expression for the thermal conductivity of the partially sintered green body can be obtained by combining Eqs. (3), (5) and (6) to give:

$$\lambda = \left(1-\frac{3}{2}v_p\right)\phi\left[\left(\frac{S'}{S}\right)\frac{1}{R'_{int}}+\left(1-\frac{S'}{S}\right)\frac{1}{R''_{int}}\right] \quad (7)$$

It is useful to regroup the terms containing $\left(\frac{S'}{S}\right)$ to yield:

$$\lambda = \lambda_0 + \left(1-\frac{3}{2}v_p\right)\phi\left(\frac{S'}{S}\right)\left[\frac{1}{R'_{int}}-\frac{1}{R''_{int}}\right] \quad (8)$$

where $\lambda_0 = \frac{\left(1-\frac{3}{2}v_p\right)\phi}{R''_{int}}$ corresponds to the green body. This achieves a description of the thermal conductivity for the partially sintered ceramic body illustrated by the idealized situation in **Fig. 2**. Even if certain aspects in this model construction can be disputed or improved, Eqs (7) and (8) describe the effects of contact area, pore volume fraction and average grain size corresponding to the successive sintering mechanisms of neck formation, densification and grain growth.

4 Results and discussion

4-1 Thermal conductivity of green bodies with different average particle sizes

For heat flow crossing the green body, the average particle size determines the number of equivalent planes in series presenting thermal resistance which should influence the thermal conductivity. The thermal conductivity values of pressed compacts of alumina powders with different average particle sizes were evaluated with laser flash measurements (table 2).

Table 2

Thermal conductivity measurements of alumina ceramic green bodies with microstructural characteristics.

Alumina powder	Pore volume fraction	Average grain size (μm)	Effective thermal conductivity ($Wm^{-1}K^{-1)}$
TM-DAR	0.45	0.16	0.42
AKP30	0.45	0.25	0.47
P172SB	0.46	0.39	0.43
P152SB	0.40	0.71	0.77
AR12	0.57	1.25	0.43
Aldrich	0.43	2.9	0.63
AC34	0.44	3.0	0.62

The porosity content fluctuations are small. Despite a large variation in grain size by almost a factor of 20, the conductivity values are restrained to the narrow range of 0.4 to 0.8 $Wm^{-1}K^{-1}$ without any particular correlation. If small grain size increases the number of equivalent planes of particle – particle contacts in the heat path, this is compensated, to a certain extent, by the

increase of parallel heat paths in a given plane through the number of contacts. This is illustrated in **Fig. 3** providing an explanation of the almost constant values of thermal conductivity of the green bodies.

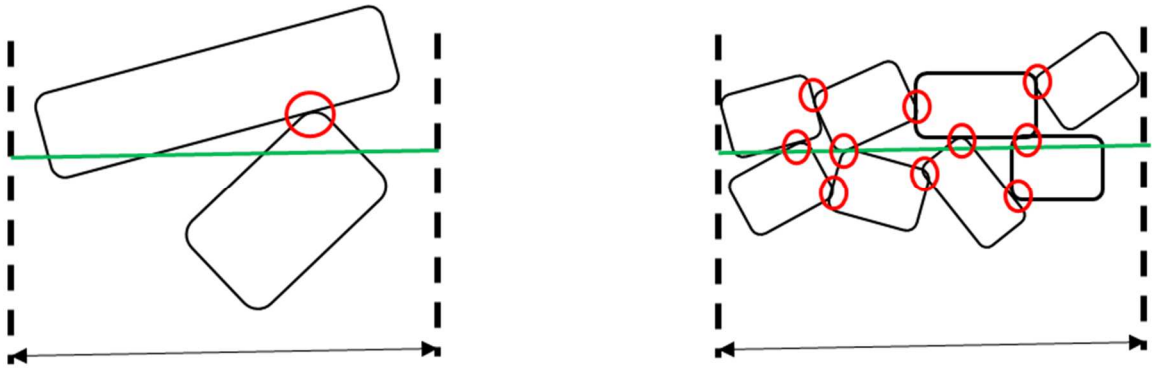

Fig. 3: Representation of two equivalent planes of contacts with the same area for green bodies with different average grain sizes.

A simple estimate of the thermal resistance of for an equivalent plane of particle – particle contacts can be made using Eq. (5) after taking into account porosity with Eq. (3). The analysis was applied to the data in table 2 and shows that the thermal resistance values for single equivalent planes of particle – particle contacts increase, approximately linearly, with grain size (**Fig. 4**).

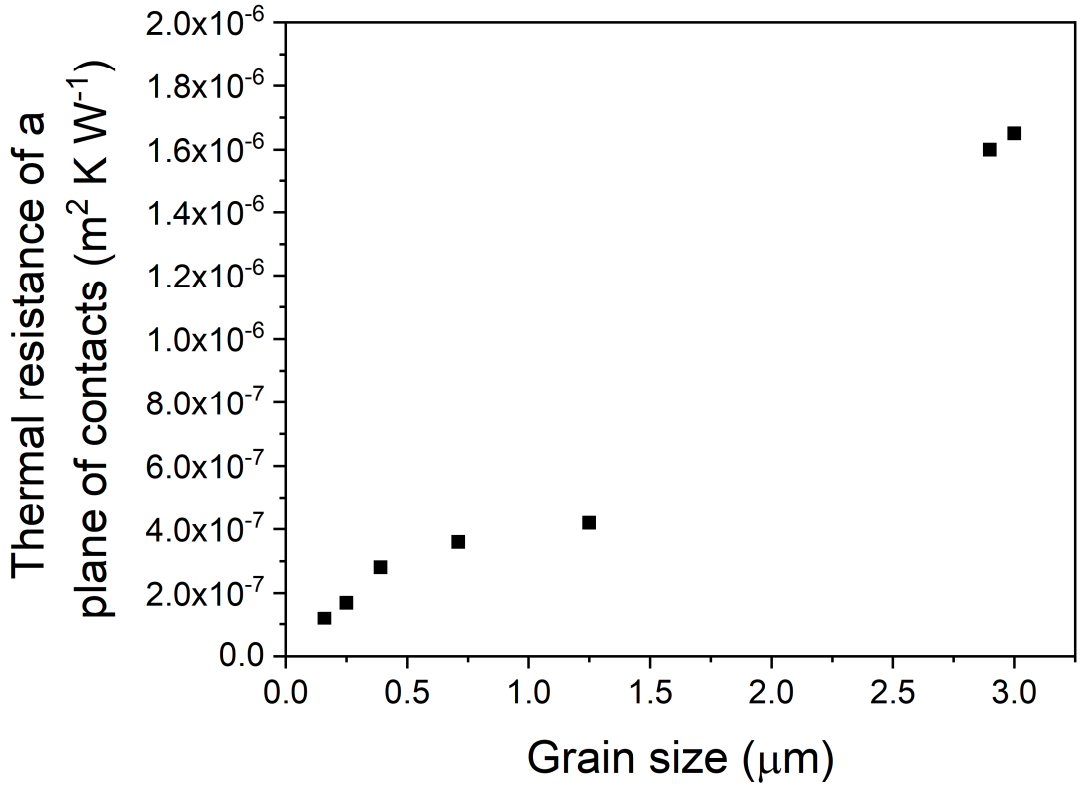

Fig. 4: Estimated thermal resistance (m^2KW^{-1}) for an equivalent plane of contacts in the green body as a function of average grain size (μm).

This is consistent with the idea that the number of heat pathways in the plane is reduced for larger grains. It can also be noted that these values are physically realistic; lying between a lower limit of a sintered grain boundary thermal resistance in alumina or other oxides at 0.6 10^{-8} m^2KW^{-1} [16, 17] and an upper limit of the thermal resistance for a mechanical contact between two metal blocks at approximately 10^{-4} m^2KW^{-1} [18].

Given that the concept of the thermal resistance for an equivalent plane of contacts in the green body is pertinent, it is now examined in more detail for heat treated green bodies (partially sintered ceramics). Two factors can contribute to its value: the actual contact area at the microscopic scale and the magnitude of interface thermal resistance within this contact area.

4-2 Particle-particle contact area in heat treated alumina green bodies

Green bodies made from the TM-DAR, AKP30 and P172SB alumina powders were heat treated at temperatures up to 1200°C. The subsequent room temperature thermal conductivity measurements are shown in **Fig. 5** and reveal a hierarchy of the curves related to average particle size.

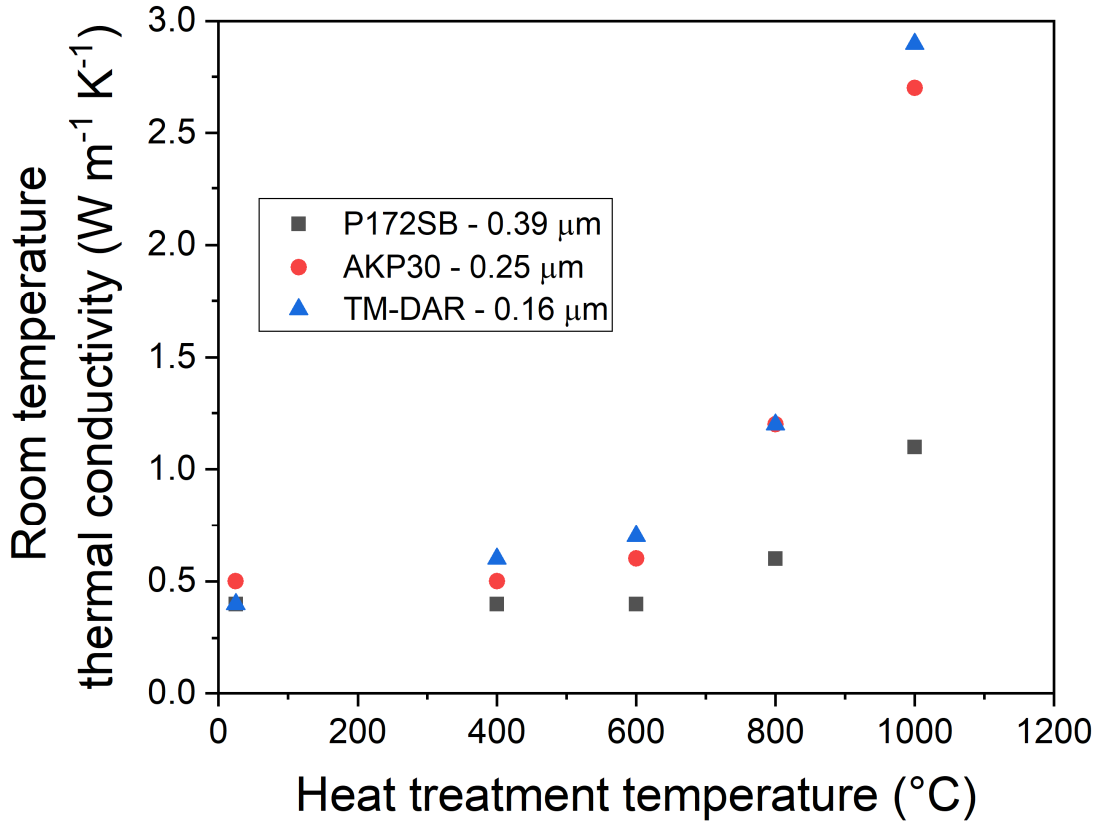

Fig. 5: Thermal conductivity at room temperature of green bodies as a function of heat treatment temperature.

For the three powders, increase in conductivity occurs for treatments above an initiation temperature in the range 400 to 600°C. However the behavior is more attenuated for the coarser P172SB powder, consistent with the reduced powder sinterability due to the granulometry. It can also be noted that for the P172SB samples a slight decrease in conductivity occurs from

0.45 $Wm^{-1}K^{-1}$ (green body) to 0.38 $Wm^{-1}K^{-1}$ when treated at 400°C. Such fluctuations can be attributed to residual humidity in the green body following earlier work [19]. For heat treatments upto 1000°C both densification and grain growth can be discounted as mechanisms significantly affecting the thermal conductivity of the green body. The dilatometric curve for the TM-DAR powder in **Fig. 6** confirms that densification is not initiated until 1000°C is attained. Furthermore the micrographs of heat treated green bodies from this same powder in **Fig. 7** do not reveal any significant grain growth until 1200°C is reached. It is therefore deduced that the conductivity change by a factor of 6 between the green body and the sample treated at 1000°C can be attributed to neck formation.

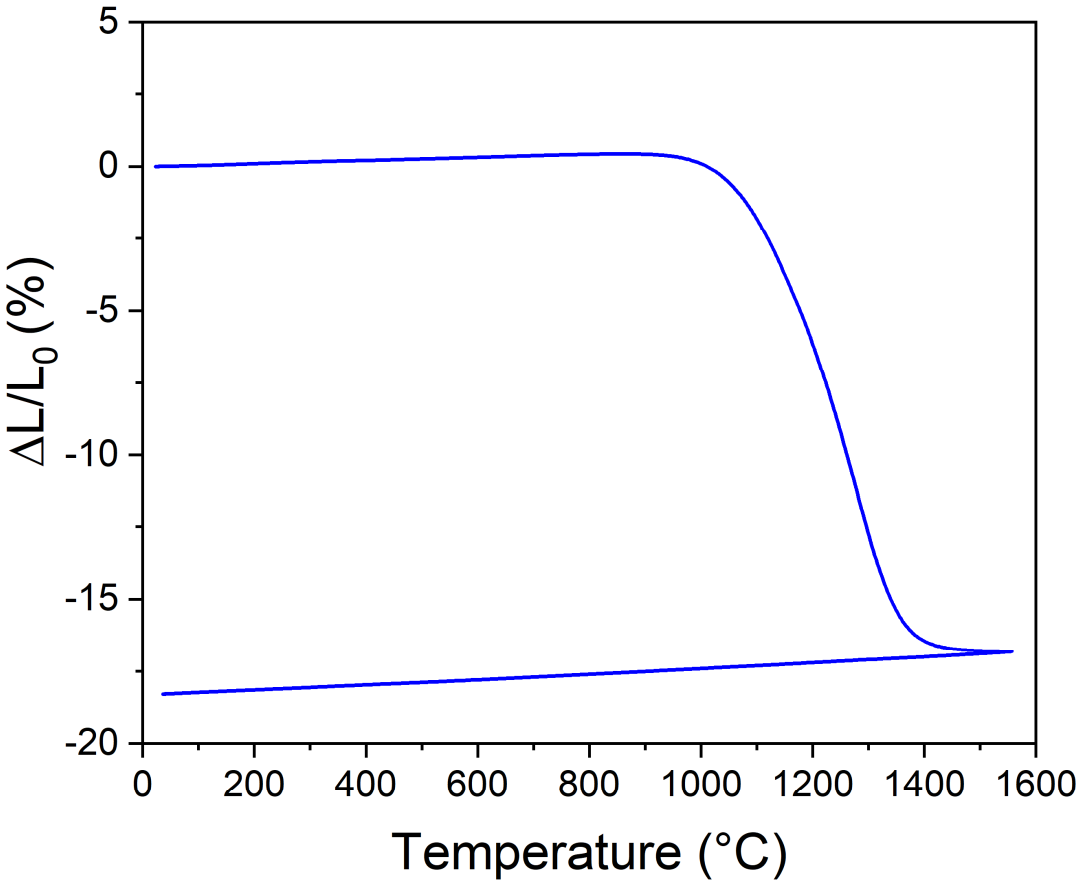

Fig. 6: Dilatometric sintering curve for TM-DAR pressed powder sample.

More information was obtained using BET measurements which are used normally to measure the specific surface area of powders. On the basis of a simple approximation [20], the method is extended to the case of green bodies. For a given particle in the green body, its external surface area divides into that proportion in contact with other particles, i.e. particle-particle interfaces, and the complementary part constituted by particle-pore interfaces. We consider the case of a granulated alumina powder (TM-DAR). The measured BET specific surface area yielded a value of 12.05 m^2g^{-1}. Then a pressed green body of this powder, broken up into mm sized chunks for BET measurements, gave a value of 12.0 m^2g^{-1}. For mm sized chunks the external surface area of the chunk is small (<0.1%) and, as an approximation, is neglected

compared to the internal surface area of the grains (particle – pore interfaces). Thus the evolution of the

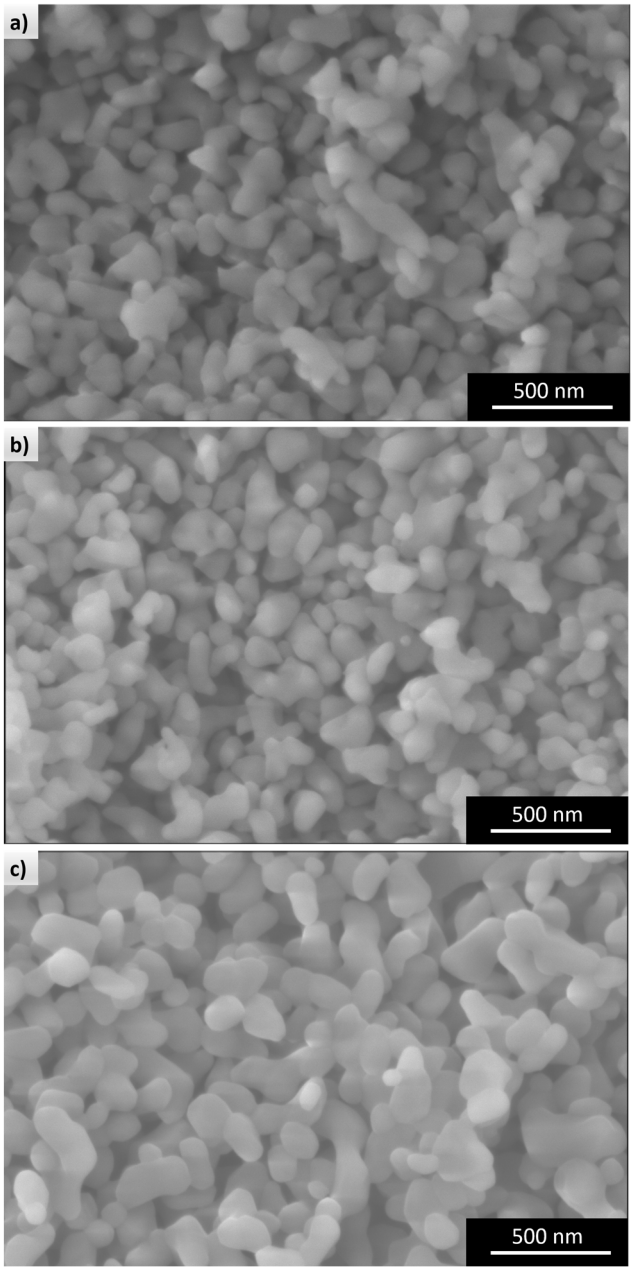

Fig. 7: Micrographs of TM-DAR green bodies treated at (a) 400°C, (b) 800°C and (c) 1200°C.

particle – particle interface area and particle – pore interface areas can be followed by BET measurements on the heat treated green bodies as shown in **Fig. 8** for the TM-DAR and AKP30 powders. It can seen in both curves there is a good correlation of decrease in BET values with increase of conductivities in **Fig. 5**, consistent with an increase of particle – particle contact area due to neck formation. Taking as an example, the TM-DAR sample fired at 1000°C yielded a value of 8.8 m^2g^{-1} compared to the green body value of 12 m^2g^{-1}. The difference between the two values is attributed to the particle-particle interfaces, expressed in the relation for the ratio ($A_{contact}$) of particle-particle contact area to total particle surface area:

$$A_{contact} = \frac{S_{green\ body} - S_{treated\ sample}}{S_{green\ body}} \quad (9)$$

where $S_{green\ body}$ is the BET specific surface area measured on the starting green body and $S_{treated\ sample}$ is the BET specific surface area for a green body thermally treated at a given temperature.

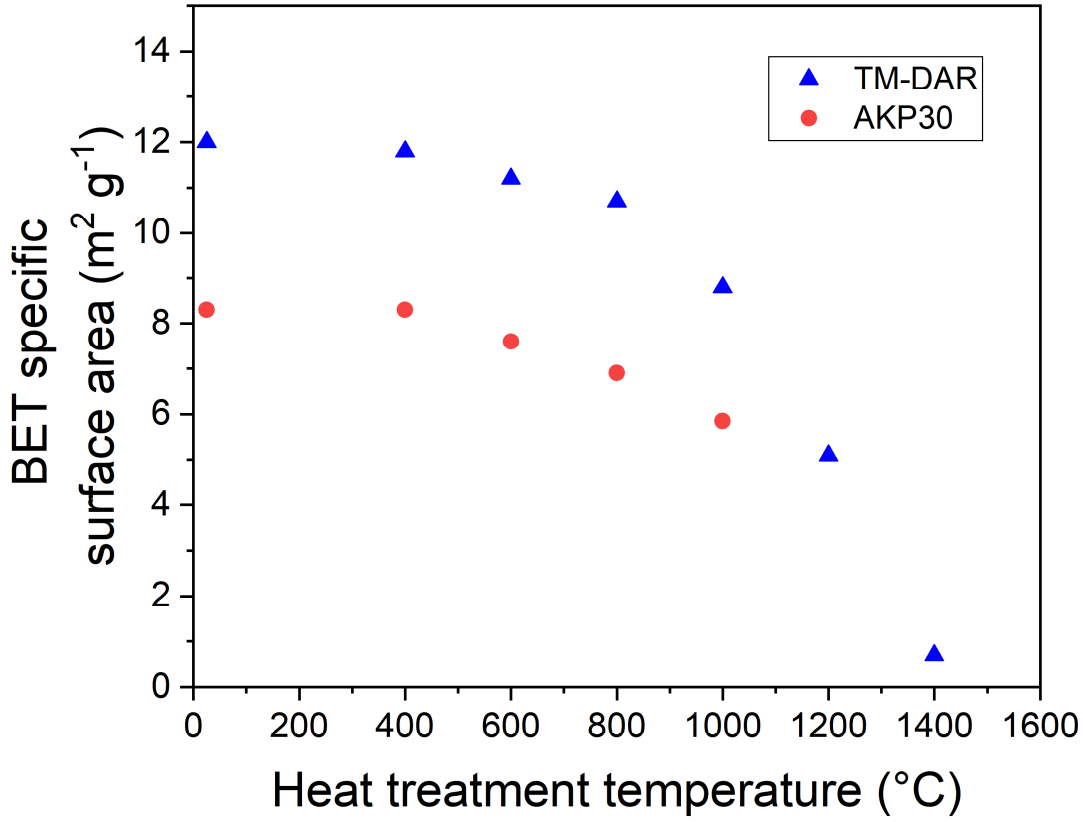

Fig. 8: BET measurements of heat treated green bodies of TM DAR (upper curve) and AKP30 (lower curve) alumina powders.

In other words, particle-particle interfaces are estimated to constitute 27% and particle-pore interfaces 73% of the original powder specific surface area. **Fig. 9** shows a plot of the thermal conductivity as a function of estimated contact area in the green body, exhibiting essentially linear behavior. This is consistent with Eq. (8) which predicts that the conductivity is proportional to the effective contact area in the equivalent planes of particle – particle contacts. The intercept with the y-axis corresponds to the thermal conductivity of the initial green body. Further support to the interpretation is given by two sets of calculations. Using the earlier approach in section 4.1 with Eq. (5) , values of the thermal resistance for an equivalent plane of contacts in the green body were calculated for different temperatures of thermal treatment. In the analysis, the particle size is taken to be 160 nm from table 1. Thus the thermal resistance of an equivalent plane of contacts (5^{th} column of table 3) is shown to decrease to a value approaching that of a sintered grain boundary of the order of 10^{-8} m^2KW^{-1} [16,17]. The second set of calculations aims to estimate the interface thermal resistance within the neck region of the contact. However it is important to point out that the BET evaluation of contact areas is 3 - dimensional whereas the notion of effective cross section of the equivalent plane is in 2 dimensions. So an unknown correcting factor maybe involved (a simple approach on an ideally packed structure of spheres suggests 2/3).

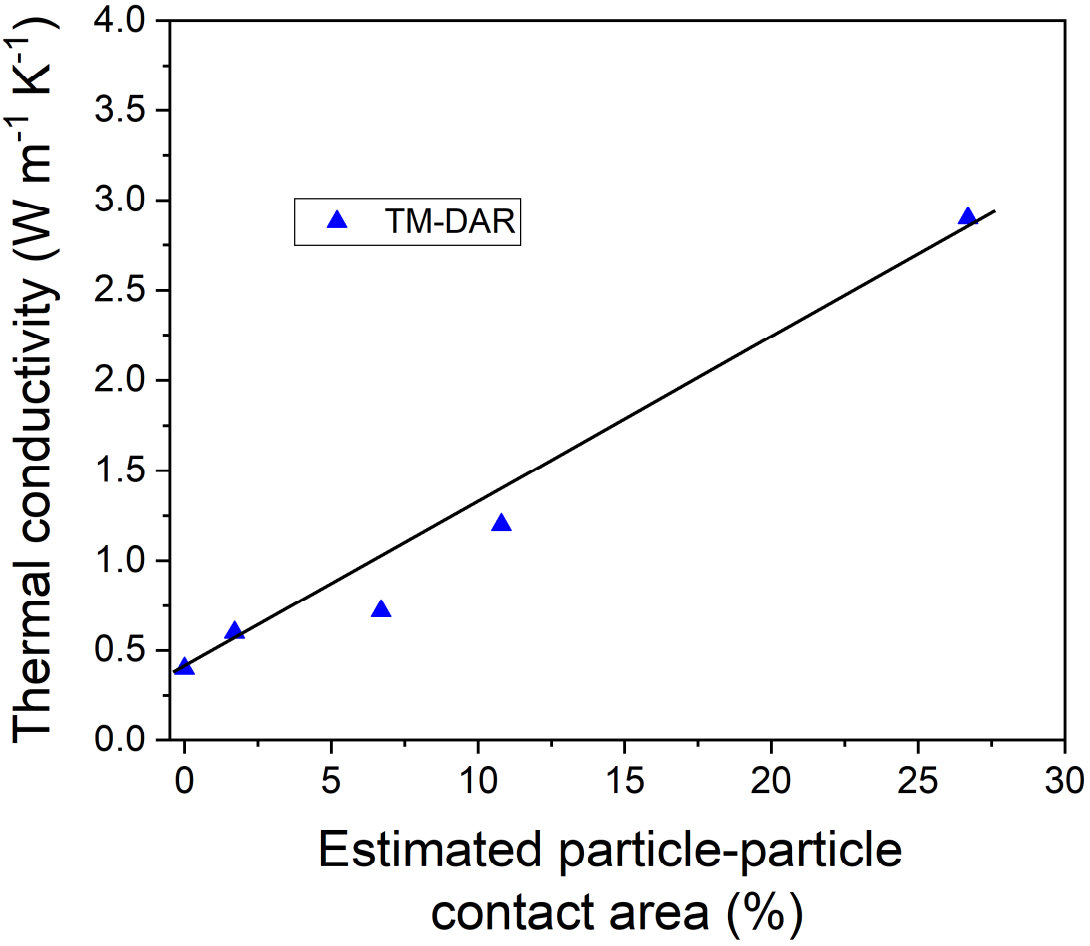

Fig. 9: Thermal conductivity of heat treated green bodies versus estimated particle – particle contact area for TM-DAR alumina powder.

Nevertheless, by solving Eq. (9) for R'_{int} which gives:

$$R'_{int} = \frac{\emptyset\left(1-\frac{3}{2}v_p\right)}{\frac{\lambda-\lambda_0}{\left(\frac{S'}{S}\right)}+\lambda_0} \qquad (10)$$

useful (approximate) values can be obtained using $\frac{S'}{S} = A_{contact}$. The estimated values for the grain boundary thermal resistance are given in the last column of table 3. With the precautions already mentioned concerning the quantitative value of the contact area, the calculated values are of the same order of magnitude as values deduced for porous alumina ceramics sintered at higher temperatures which are in the range 0.6 10^{-8} to 2.0 10^{-8} m^2KW^{-1} [16]. A representative value of R'_{int} was also be obtained from the slope in **Fig. 9** yielding 0.55 10^{-8} m^2KW^{-1}. It is interesting to note that a slight curvature upwards can be detected as temperature of thermal treatment increases which would correspond to decrease in R'_{int}. Such behaviour could be elegantly explained by elimination of the more resistive higher energy grain boundaries as sintering progresses to higher temperatures.

Table 3

Calculations of overall contact plane thermal resistance (Eq.(5)) and estimates of local sintered contact thermal resistance (Eq. (10)) for TM-DAR alumina green bodies treated at different temperatures.

Thermal treatment temperature (°C)	Pore volume fraction	Estimated contact area (%)	Measured thermal conductivity ($Wm^{-1}K^{-1}$)	Overall thermal resistance of contact plane (m^2KW^{-1})	Estimated thermal resistance of sintered contacts at local scale (m^2KW^{-1})
25	0.45	-	0.4	$1.3\ 10^{-7}$	
400	0.44	0.017	0.6	$8.7\ 10^{-8}$	$4.3\ 10^{-9}$
600	0.45	0.067	0.7	$7.4\ 10^{-8}$	$1.1\ 10^{-8}$
800	0.45	0.108	1.2	$4.3\ 10^{-8}$	$6.7\ 10^{-9}$
1000	0.44	0.267	2.9	$1.8\ 10^{-8}$	$5.3\ 10^{-9}$

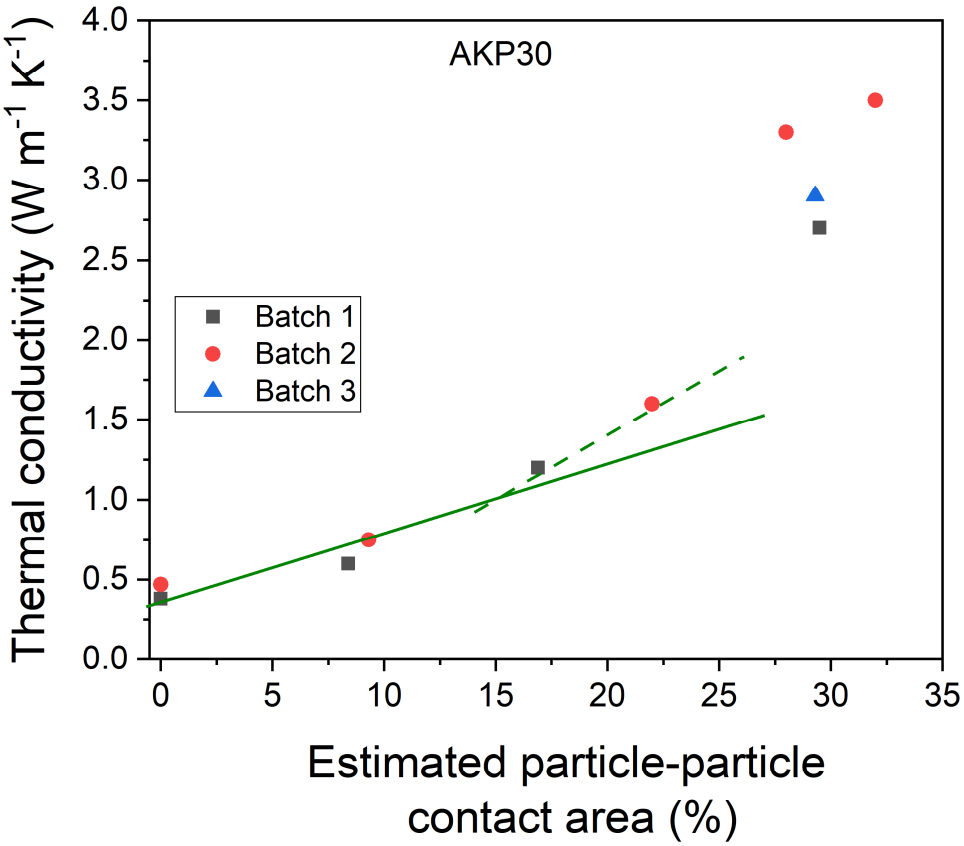

Fig. 10: Thermal conductivity versus estimated particle – particle contact area of partially sintered green bodies of AKP30 alumina powder. The two lines correspond to a change of grain boundary thermal resistance from $1.9\ 10^{-8}$ m^2KW^{-1} to $1.0\ 10^{-8}$ m^2KW^{-1} as the necks form in the green body. Squares, full circles and the triangle correspond to three different batches of samples.

A similar trend was observed for the AKP30 series as shown in **Fig. 10** with a decrease in estimated thermal resistance for the sintered contact regions from 1.9 10^{-8} m^2KW^{-1} to 1.0 10^{-8} m^2KW^{-1}. In fact, the results shown in Fig. 10 come from three different batches of samples made with the AKP30 powder. This gives a visual impression of the reproducibility of the approach; related to the error bars in values for conductivity (< ±5%) and BET measurements (< ±2%) but also sample fabrication including thermal treatment. Pore volume fraction variation for these samples is in the range 0.43 to 0.45.

As a last point of discussion, it is interesting to envisage how the thermal conductivity of the ceramic green body would evolve with temperature in a thermal treatment for firing. The model, as developed so far, describes the increase that occurs due to microstructural changes of neck formation, densification and eventually grain growth. It ignores with the approximation made in Eq. (5), the dependence of intrinsic conductivity on temperature which for crystalline dielectric solids like alumina should decrease. This should be sufficient for an intitial temperature range when the equivalent plane of contacts dominates the response. However the microstructural changes will saturate at some point in the firing cycle and no longer mask variation in the intrinsic thermal conductivity. A more complete treatment should take this aspect into account for numerical modelling of the green body behaviour during firing.

5. Conclusions

The concept of equivalent planes of contacts has been introduced to describe the thermal resistance of a green body. These planes, oriented perpendicular to the heat flow direction, are considered to be separated by the average particle size. In practice the equivalent plane can be attributed with a certain width to accommodate contacts just above and below the plane. Experimentally the thermal resistance for an equivalent plane of contacts in the green body increases with particle size, explained by a reduced number of contacts in the plane.

In the situation where the thermal resistance of the grains (intrinsic thermal conductivity) is much smaller than that of an equivalent plane of contacts, a simplified model has been developed to describe the effects of pore volume fraction, average particle size and the contact area between particles on the thermal conductivity of green or partially sintered ceramic. By using BET specific surface area measurements to estimate the contact area between particles due to neck formation, this relation has been tested on partially sintered alumina ceramics fired at temperatures from 400°C to 1200°C. Both theory and experiment confirm a strong increase in thermal conductivity from 0.4 $Wm^{-1}K^{-1}$ to > 3 $Wm^{-1}K^{-1}$. On the basis of the model, estimates of the grain boundary thermal resistance in the sintered contact area are of the order of 10^{-8} m^2KW^{-1}, consistent with other studies. It can be noted that this value decreases for the higher temperature treatments, suggesting that the more resistive higher energy grain boundaries are eliminated as sintering progresses.

Finally, this information on the thermal conductivity evolution due to neck formation is relevant as input data for numerical modelling of the green body behaviour during thermal treatment [21] as well as for sintering studies.

References

1. T. Olorunyolemi, A. Birnboim, Y Carmel, O.C. Wilson Jr., I .Knowlton Lloyd. S. Smith, R. Campbell, "Thermal conductivity of zinc oxide: from green to sintered state", J. Am. Ceram. Soc. **85**, 1249-1253 (2002).
2. C. Poulier, D.S. Smith, M. Viana, J. Absi, "Thermal conductivity of pressed powder compacts: tin oxide and alumina", J. Eur. Ceram. Soc. **27**, 475-478 (2007).
3. D.S. Smith, S. Fayette, S. Grandjean, C. Martin, R. Telle and T. Tonnesen, "Thermal Resistance of Grain Boundaries in Alumina Ceramics and Refractories", J. Am. Ceram. Soc. **86** (2003) 105-111.
4. C. Poulier, D.S. Smith, M. Viana, J. Absi, "Evolution of thermophysical characteristics in tin oxide: from pressed powder compact to fired porous body", J. Am. Ceram. Soc. **91**, 965-969 (2008).
5. F. Raether, R. Springer, "In-situ measurement of neck formation during sintering of alumina by a novel thermo-optical measuring device", Advanced Engineering Materials **2**, 741-744 (2000).
6. R.L. Coble, "Initial sintering of Alumina and Hematite", J. Am. Ceram. Soc. **41**, 55-62 (1958)
7. A. Birnboim, T. Olorunyolemi, Y. Carmel, "Calculating the thermal conductivity of heated powder compacts", J. Am. Ceram. Soc. **84**, 1315-1320 (2001).
8. T. Uhlirova, V. Necina, W. Pabst, "Modeling of Young's modulus and thermal conductivity evolution of partially sintered alumina ceramics with pore shape changes from concave to convex", J. Eur. Ceram. Soc. **38**, 3004-3011 (2018)
9. W. Pabst and E. Gregorova, "Minimum solid area models for the effective properties of porous materials – a refutation", Ceramics – Silikaty **59** (3), 244-249 (2015).
10. R.W. Rice, "Evaluation and extension of physical property – porosity models based on minimum solid area", J. Mat. Sci. **31**, 102-118 (1996).
11. O. Knacke, O. Kubaschewski, K. Hesselmann, Thermal chemical properties of inorganic substances 2nd edition Berlin : Springer Verlag 1976.
12. A. Degiovanni, "Thermal diffusivity and flash method", Rev. Gen. Therm. **16** (185), 420-441 (1977).
13. J. A. Cape and G.W. Lehman, "Temperature and finite pulse – time effects in the flash method for measuring thermal diffusivity", J. Appl. Phys. 34 (1963) 1909-1913.
14. R. Landauer, "The electrical resistance of binary metallic mixtures", J. Appl. Phys. **21** (1952) 779-784.
15. D.S. Smith, A. Alzina, J. Bourret, B. Nait-Ali, F. Pennec, N. Tessier-Doyen, K. Otsu, H. Matsubara, P. Elser and U.T. Gonzenbach, "Thermal conductivity of porous materials", J. Mater. Res. **28** (2013) 2260-2271.
16. D.S. Smith, F. Puech, B. Nait-Ali, A. Alzina, S. Honda, "Grain boundary thermal resistance and finite grain size effects for heat conduction through porous polycrystalline alumina", Int. J. Heat and Mass Transfer **121** (2018) 1273-1280.
17. H.S. Yang, G.R. Bai, L.J. Thompson, J.A. Eastman, "Interfacial thermal resistance in nanocrystalline yttria-stabilized zirconia", Acta. Mater. **50** (2002) 2309-2317.

18. J.P. Holman, *Heat Transfer*, 6th edition, pp.55-58. McGraw-Hill Book Co., New York 1986.
19. B. Nait-Ali, S. Oummadi, E. Portuguez, A. Alzina, D.S. Smith, "Thermal conductivity of ceramic green bodies during drying", J. Europ. Ceram. Soc. **37** (2017) 1839-1846.
20. R.M. German and Z.A. Munir, "Surface area reduction during isothermal sintering", J. Am. Ceram. Soc. **59** (1976) 379-383.
21. F.G. Raether, "Current state of *in situ* measuring methods for the control of firing processes", ", J. Am. Ceram. Soc. **92** (2008) S146 – S152.